PHYSICAL REVIEW B **93**, 014201 (2016)

Structural changes during a liquid-liquid transition in the deeply undercooled $Zr_{58.5}Cu_{15.6}Ni_{12.8}Al_{10.3}Nb_{2.8}$ bulk metallic glass forming melt

Moritz Stolpe,[1] Isabell Jonas,[2] Shuai Wei,[3] Zach Evenson,[2,4] William Hembree,[1] Fan Yang,[2] Andreas Meyer,[2] and Ralf Busch[1]
[1]*Chair of Metallic Materials, Department of Material Science and Engineering, Saarland University, 66123 Saarbrücken, Germany*
[2]*Institute for Materials Physics in Space, German Aerospace Center (DLR), 51147 Cologne, Germany*
[3]*School of Molecular Science, Arizona State University, Tempe, Arizona 85287, USA*
[4]*Heinz Maier-Leibnitz Zentrum (MLZ) and Physik Department, Technische Universität München, Lichtenbergstrasse 1, 85748 Garching, Germany*

(Received 24 July 2015; revised manuscript received 15 December 2015; published 13 January 2016)

Using high energy synchrotron x-ray radiation combined with electrostatic levitation, *in situ* structural analysis of a bulk metallic glass forming liquid is performed from above the liquidus temperature down to the glass transition. The data indicate a liquid-liquid transition (LLT) in the deeply undercooled state at $T/T_g \sim 1.2$ which manifests as a maximum in the heat capacity and an abrupt shift in the first peak position of the total structure factor in the absence of a pronounced density change. Analysis of the corresponding real-space data shows that the LLT involves changes in short- and medium-range order. The structural changes on the length scale of medium-range order imply a fragile-strong transition in agreement with experimental viscosity data.

DOI: 10.1103/PhysRevB.93.014201

I. INTRODUCTION

Within the last decades increasing evidence for polymorphous phase transitions in the liquid state, referred to as liquid-liquid transitions (LLTs), has been reported experimentally [1–3] as well as computationally [4–7]. These findings include the liquid [2,7,8] as well as its frozen-in glassy state [9] and span a wide range of chemical species including, e.g., water [10,11], aqueous solutions [12], Y_2O_3-Al_2O_3 [1], SiO_2 [7], BeF_2 [13], thriphenyl phosphite [14,15], Si, P [2,8], Ge [3], and recently multicomponent bulk metallic glass (BMG) forming systems (Ce-Al [9], Zr-Cu-Ti-Ni-Be [16]).

Aside from the fundamental question of whether a system that is characterized by permanently rearranging configurations can exist in distinct modifications (liquid phases) that are equal in composition but differ in local structure and thermodynamic properties [17], LLTs are also of interest due to their implications on the system's dynamics. In particular, LLTs have been proposed to explain experimentally observed anomalous changes in liquid dynamics, a phenomenon known as fragile-strong transition (FST) [7,16,18–20]. Apart from their relevance to fundamental aspects of physics, FSTs are recently recognized for their technological importance, e.g., in phase-change memory applications [21,22]. The sensitivity of liquid dynamics with respect to temperature changes is commonly quantified by the concept of "fragility" [23]. Liquids that follow a near exponential temperature dependence (Arrhenius behavior) are classified as "strong," while liquids that deviate from Arrhenius behavior are defined as "fragile." Often, experimental data are best described by the empirical Vogel-Fulcher-Tamman (VFT) equation

$$f = f_0 \exp[D^* T_0/(T - T_0)], \tag{1}$$

where D^* and T_0 are system-specific parameters, f denotes a dynamical variable (e.g., diffusivity, viscosity, or relaxation time), f_0 is the lower limit for $T \to \infty$, T_0 is the temperature where f would approach infinity in the limit $T \to T_0$, and D^* is the so-called fragility parameter. Strong liquids are characterized by larger values of D^* and T_g/T_0, fragile liquids exhibit lower D^* and T_g/T_0 (T_g is the glass transition temperature). In this description a FST manifests in changes in D^* and T_g/T_0.

A connection between the dynamics and thermodynamics can be achieved via the Adam-Gibbs-relation [24]

$$f = f_0 \exp(B/T S_C), \tag{2}$$

where B is an effective activation energy barrier usually obtained from data fitting [25]. In this model, the fundamental quantity that drives the evolution of the system's dynamics is the configurational entropy S_c, which gives a measure of the number of configurational states that the system can access in its potential energy landscape [26,27]. Though the theoretical basis of the Adam-Gibbs entropy model [24] has been questioned [28] the general applicability of Eq. (2) is corroborated by the strong empirical correlation between the fragility and the evolution of excess entropy of the liquid over the crystalline phase S_{ex} of a large number of glass forming systems [29,30]. Expecting that the structural changes occurring during a LLT manifest themselves in the thermodynamics via a change in S_c, Eq. (2) provides a qualitative link to the resulting changes in the liquid's dynamics.

Here we report on the structural changes of a bulk metallic glass forming alloy from far above the melting point down to the glass transition. A LLT in the deeply supercooled liquid is revealed at $T/T_g \sim 1.2$ which manifests as an anomalous shift in the first peak position of the static total structure factor $S^*(Q)$. We further show that the LLT is thermodynamically reflected by a peak in the ratio of specific heat capacity to total hemispherical emissivity c_p/ε, denoting a decrease in entropy associated with the atomic reconfiguration. Relying on a previously established empirical correlation linking the structural changes on a length scale of about 3 to 4 atomic diamters (~1 nm) to fragility [31], we demonstrate that this change in local liquid structure implies a FST, thus explaining the experimentally observed difference in fragility between the high and low temperature viscosity behavior of a number of BMG liquids [32]. The current experimental findings

corroborate that FSTs may arise from an underlying phase transition in the liquid state as postulated earlier within the big picture of glass forming liquids [19].

II. EXPERIMENTAL METHODS

To detect and explore the structural changes associated with a LLT we performed *in situ* high energy synchrotron x-ray diffraction (HESXRD) on electrostatic levitated (ESL) droplets of the $Zr_{58.5}Cu_{15.6}Ni_{12.8}Al_{10.3}Nb_{2.8}$ BMG forming liquid. HESXRD was carried out at Petra III P07 beamline at DESY (Hamburg). This technique is appropriate for time-resolved structural studies on the atomic scale. The ESL technique allows access to the deeply undercooled liquid, due to the absence of container walls, which may act as preferential nucleation sites [33]. For a detailed description of the experimental setup and data analysis the reader is referred to the Supplemental Material [34].

III. RESULTS AND DISCUSSION

The selected alloy possesses a relatively low critical cooling rate for glass formation (1.75 K/s) [35], which makes it particularly ideal for structural investigations over a wide temperature range from above the liquidus T_l down to the glass transition temperature T_g. Moreover, this alloy melt shows a discrepancy between the high and low temperature viscosity behavior, which has been proposed to be related to a FST [32].

The temperature-time profile obtained during free cooling of the levitated molten droplet is shown in Fig. 1(a). Within the temperature range from 1473 to 673 K no recalescence due to bulk crystallization of the sample is observed. Note that 673 K is the lower detection limit of the pyrometer used within this study. Figure 1(b) shows a density versus temperature plot obtained from a separate volume measurement in the ESL under similar experimental conditions. During undercooling towards the glass transition T_g, the density increases continuously without any evidence of a sudden change that would indicate crystallization. The evolution of the total structure factor $S^*(Q)$ during cooling into the glass is shown in Fig. 1(c). At all temperatures, $S^*(Q)$ reveals the typical appearance of an amorphous structure lacking long-range order. During undercooling, the maxima of $S^*(Q)$ sharpen and gain in intensity reflecting the less pronounced thermally induced smearing of atomic correlations. However, the patterns do not show any evidence for crystallization. No Bragg peaks are visible in the entire temperature and Q range of the investigation. Moreover, inspection of the measured two-dimensional (2D) detector patterns reveals no indications of the formation of crystallites.

To reveal a possible phase transition in the liquid state, the evolution of the total static structure factor $S^*(Q)$ with temperature is analyzed [16,37]. In Fig. 2(a) the position of the first maximum in $S^*(Q)$, $Q_{1\max}$, is plotted during heating at 100 K/min from an initially glassy sample and subsequent free cooling from the equilibrium liquid. For clarity the data of the crystallized material (gap in heating data) is not displayed. During heating, $Q_{1\max}$ decreases as expected for an increase of interatomic distances with decreasing density [38]. At about 770 K, the sample crystallizes in agreement with differential

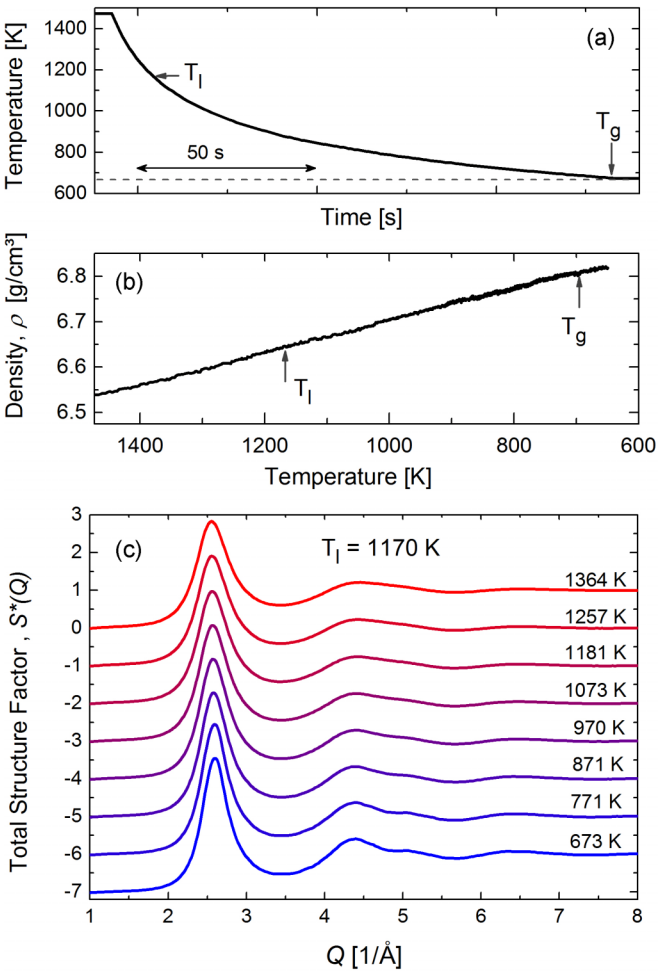

FIG. 1. (a) Time-temperature profile for free cooling of the sample in ESL. (b) Density as a function of temperature during cooling into the glassy state. (c) Evolution of the static total structure factor $S^*(Q)$ during undercooling the levitated molten droplet into the glassy state for the temperature profile shown in (a).

thermal analysis [39]. Above the melting point T_m, $Q_{1\max}$ once again decreases with increasing T. However, a linear extrapolation of the low temperature supercooled liquid data ($T < 800$ K) does not match the high temperature data ($T > T_m$). Upon subsequent cooling, $Q_{1\max}$ first follows the heating data until a sudden increase occurs in the deeply undercooled liquid between 900 and 800 K. As a result, the values of $Q_{1\max}$ match those obtained during previous heating. To further exclude that the shift of $Q_{1\max}$ results from the formation of crystallites, the changes in the diffraction intensity $\Delta I_{\mathrm{LLT}}(Q)$ are compared with the changes associated with the initial stage of crystallization $\Delta I_{\mathrm{cryst}}(Q)$. Both are found to be substantially different (see Fig. 3) corroborating that the observed behavior of $S^*(Q)$ is the signature of a structural transition within the deeply undercooled liquid state and does not correspond to the onset of crystallization of the melt.

The aforementioned findings imply a thermodynamic signature associated with a reorganization of the atomic structure. Using the Stefan-Boltzmann law, c_p/ε is calculated from the temperature-time profiles during cooling [Fig. 1(a)] and shown in Fig. 2(b) in comparison to literature data obtained from

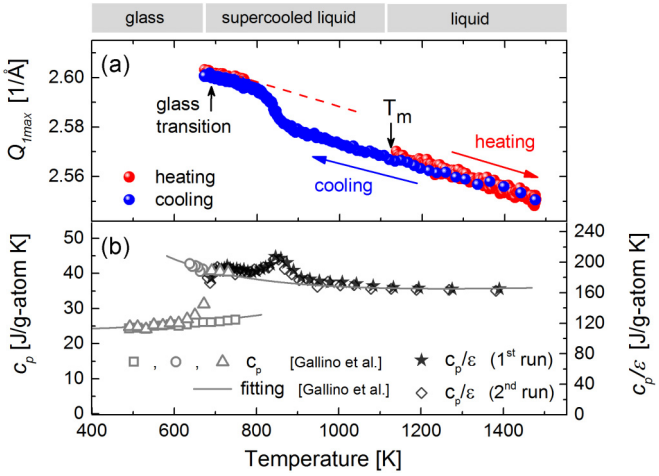

FIG. 2. (a) Position of the first maximum of $S*(Q)$, $Q_{1\max}$, during heating of an initially glassy sample and subsequent cooling down to the glassy state. (b) Ratio of specific heat capacity to total hemispherical emissivity c_p/ε calculated from the temperature profile measured in ESL [Fig. 1(a)] during cooling to the glassy state in comparison with the measured calorimetric c_p data of Gallino *et al.* [36].

calorimetric measurements [36]. In contrast to the expected course predicted from fitting of the c_p data close to T_g [36], the measured c_p/ε passes through a maximum coinciding with the observed anomaly in $S*(Q)$ and is therefore regarded as the thermal signature associated with the transition in the deeply undercooled liquid. Taking $\varepsilon = 0.22$ for temperatures around T_g, as deduced from the comparison of c_p/ε with the calorimetric c_p in Fig. 2(b), the additional heat release obtained from integration of the peak is ∼0.5 kJ/g atom, and corresponds to a decrease in entropy of ∼0.6 J/g atom K, i.e.,

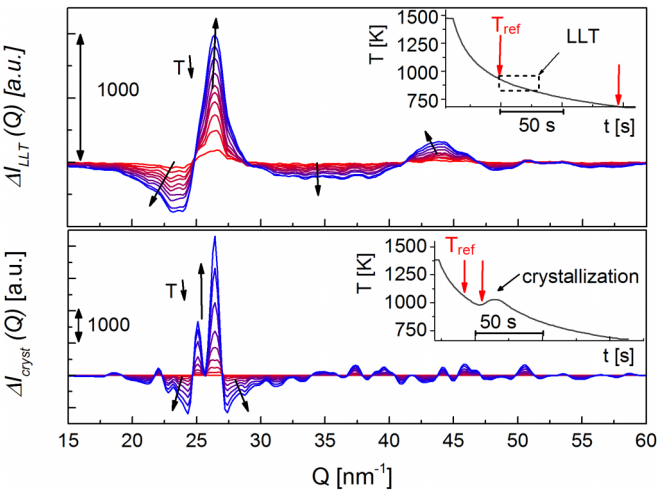

FIG. 3. Changes in diffraction patterns $I(Q)$, associated with the LLT, $\Delta I_{\mathrm{LLT}}(Q)$ (upper part), and with the initial stage of crystallization $\Delta I_{\mathrm{cryst}}(Q)$ (lower part). Changes are determined with respect to a reference temperature T_{ref} to amplify the changes associated with each process. Insets show the corresponding temperature-time profiles of the sample. The reference temperatures and the temperature range used for the comparison are indicated by arrows in the inset.

∼7% of the entropy of fusion [36] in good agreement with the values measured earlier for a LLT in another bulk metallic glass former [16]. This is consistent with an increase in order during the transition, i.e., a transition from a less ordered high temperature (HTL) to a more ordered low temperature liquid phase (LTL). The appearance of peaklike anomalies in c_p/ε and volumetric thermal expansion coefficient α for the current alloy has been previously reported [40]. Lacking diffraction data, however, those observations were attributed to crystallization [40], which is not supported by the current structural analysis. The large scattering observed in the present analysis of α (see Supplemental Material [34]) does not allow one to draw conclusions about an anomaly as observed in Ref. [40]. However, the continuous linear change of density with temperature [Fig. 1(b)] indicates that there is no significant change in density or α associated with LLT.

In the following we make use of the Fourier transforms of $S*(Q)$ and analyze the evolution of the associated total radial distribution function $G(r)$. We note that the total structure factor of a five component alloy is the sum of 15 partial structure factors, which prevents a detailed structural analysis. Nevertheless, we will show that the $G(r)$ data are basically in accordance with a structural transition as indicated by the evolution of thermodynamics and structure in reciprocal space. Furthermore, the calculated $G(r)$ will enable us to connect the structural changes to the dynamics.

Figure 4 shows the evolution of $G(r)$ during cooling from 1473 K, i.e., about 300 K above the liquidus, down 673 K. Arrows indicate the shift of maxima and minima with decreasing temperature. A close up view of the first two peaks corresponding to interatomic correlations at the length scale of SRO is shown in the inset. With lower temperatures, at all length scales, the peaks sharpen and gain in intensity reflecting the higher interatomic correlations resulting from the increasing spatial confinement and less pronounced thermal vibrations of the atoms.

Figure 4(b) shows the evolution of the first five peak positions r_i and peak intensities $G(r_i)$ normalized to their value at 673 K upon cooling from the equilibrium liquid down to the glass. Several anomalies, involving the length scale of SRO and MRO, can be detected. For instance, r_1 shows an unexpected change in slope, r_4 and r_5 display steplike decreases, while $G(r_4)$ and $G(r_5)$ exhibit abrupt increases upon undercooling. Magnified plots showing the individual courses of r_i and $G(r_i)$ during cooling can be found in the Supplemental Material [34]. The anomalies in real space data coincide exactly with the shift of $Q_{1\max}$ and the c_p/ε peak as illustrated by the shaded region, suggesting a direct connection between these observations. We note that the anomalous, negative expansion of r_1 is a common observation in metallic melts and its origin has been debated recently [41–43]. Figure 4 further reveals a diverse structural evolution at different length scales which may explain the absence of a pronounced density change during the LLT [cf. Fig. 1(c)]. The absence of a marked density change throughout a LLT in another bulk metallic glass forming melt was already observed earlier [16]. In this connection we emphasize that the metallic bonding character, energetically, does not prefer considerably less efficiently packed structures as compared to systems that are dominated by directional bonding. It thus

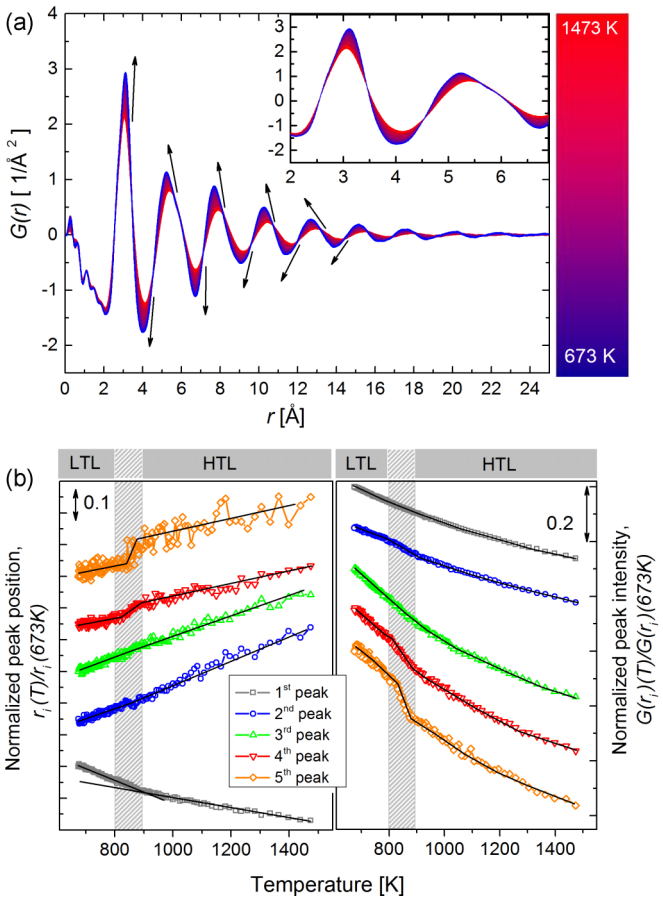

FIG. 4. (a) Evolution of $G(r)$ during undercooling the levitated droplet from above the melting point down into the glass. The inset shows a close up view of the first two peak positions. Arrows indicate the evolution of peak maxima and minima with decreasing temperatures. (b) Evolution of the first five peak positions $r_i(T)/r_i(673\ \mathrm{K})$ and peak intensities $G(r_i)/G(r_i)(673\ \mathrm{K})$ normalized to their value at 673 K. LTL: low temperature liquid; HTL: high temperature liquid. The shaded region indicates the LLT. Solid lines are to guide the eyes only. Curves are shifted for clarity. Magnified plots of the individual course of peak positions and heights can be found in the Supplemental Material [34].

appears that in these multicomponent metallic systems the transition from one densely packed liquid phase to another is driven by chemical ordering tendencies resulting from the large negative heat of mixing among the constituents.

The above findings imply that the LLT involves structural changes including SRO (cf., e.g., r_1) and MRO (cf., e.g., r_4 and r_5). Numerical and experimental findings indicate that energetically preferred, more efficiently packed atomic clusters (EPCs)—exemplarily but not necessarily icosahedra—are locally favored structures associated with SRO in metallic liquids [44–47]. Moreover, molecular dynamics studies suggests that EPCs can aggregate, building up larger (e.g., networklike) structural units, which, in turn, are associated with the viscous slowdown during undercooling [48–52]. Due to their lower degeneracy of states [46], the formation of locally favored structures (ECPs or agglomerates) is accompanied by an increase in order. Thermodynamically, an increasing ordering tendency upon cooling manifests as a rise in c_p as T_g is approached [46,50].

Although the direct observation of a dynamic crossover via conventional viscometry in the present alloy is precluded by crystallization, in the following we demonstrate that the observed structural changes imply a FST, giving an explanation for the difference in fragility observed between the high and low temperature viscosities. To validate that the atomic-scale structural changes are in agreement with a FST, we apply a recently established empirical correlation that links fragility to the evolution of atomic correlations on length scales of about 1 nm (MRO) [31]. Alternatively, a correlation linking the high temperature viscosity of metallic melts to the evolution of the first peak height in $S^*(Q)$ was proposed recently [53]. However, based on its derivation, this relation is unable to explain the experimentally observed diversity of the fragility of metallic liquids at lower temperatures near T_g and, hence, is not used in the present study. The applied correlation [31] links fragility to a structural metric defined as

$$\delta = \frac{\Delta V_{4-3}(T)}{V_{4-3}(T_g')} = \frac{V_{4-3}(T) - V_{4-3}(T_g')}{V_{4-3}(T_g')},$$

which as a first approximation was interpreted as the temperature-induced structural dilatation on a length scale of about 3 to 4 atomic diameters (∼1 nm) [31]. The volume enclosed between the third and fourth peak position of $G(r)$, r_3 and r_4, is denoted as $V_{4-3}(T) = 4/3\,\pi[r_4(T)^3 - r_3(T)^3]$, and T_g' is the temperature where the systems structurally enters its supercooled liquid state when heated through the glass transition [31]. Considering that cluster-based structural models for metallic glasses estimate the extent of locally dense-packed cluster aggregates to be of the order of 1 nm [54], and taking into account that the expansion of MRO through an aggregation or network formation of ECPs is thought to be related to the viscous slowdown [48,49,51,52], it is justifiable to assume that fragility is inherently linked to structural changes on this length scale. In particular, it was found that a larger δ corresponds to a more fragile behavior [31], and vice versa, as shown in Fig. 5(a) for seven different bulk metallic glass formers. The negative of the slope of δ in Fig. 5(a) corresponds to the structural fragility parameter $m_{\mathrm{str}}^{(V_{4-3})}$, which is plotted against the fragility steepness index m in Fig 5(b). Note that $m_{\mathrm{str}}^{(V_{4-3})}$ scales linearly with m and can be converted into D^* values via $m = 16 + 590/D^*$ [55]. In accordance with Ref. [31], δ is calculated from the temperature dependence of r_3 and r_4 (Fig. 3) and its negative value is plotted on a T_g'-scaled inverse temperature plot in Fig. 5(c). It is evident that the high temperature liquid (HTL) and the low temperature liquid (LTL) vary significantly in terms of δ. In the HTL, δ noticeably decreases upon cooling, as expected for a more fragile liquid [31]. In contrast, below the LLT, δ remains almost constant, fluctuating around zero, as is characteristic for kinetically stronger behavior [31]. Making use of the linear correlation depicted in Fig. 5(b), the slope $m_{\mathrm{str}}^{(V_{4-3})}$ of the HTL is converted into m and D^* values. This yields a change from $D^*_{(\mathrm{LTL})}{}^{\mathrm{expt}} = 21$ for the LTL [32] to $D^*_{(\mathrm{HTL})} = 12$ for the HTL which is close to the value obtained from Couette-viscometry $D^*_{(\mathrm{HTL})}{}^{\mathrm{expt}} = 10$ [32]. Our analysis

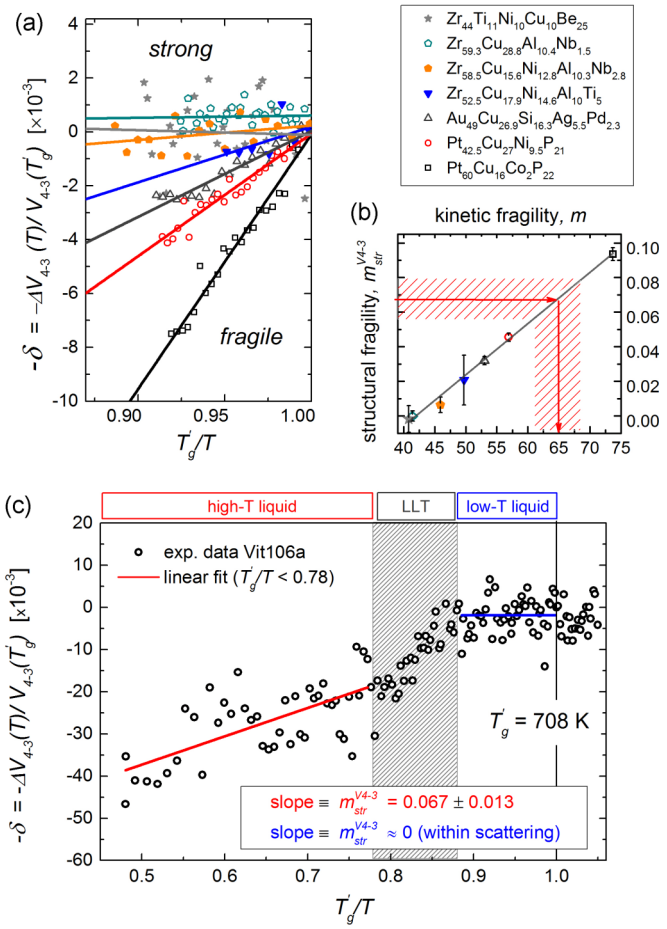

FIG. 5. (a) Temperature-induced changes in V_{4-3}, ΔV_{4-3}, with respect to its value at T_g' plotted versus T_g'/T for seven bulk metallic glass forming alloys. Note that the negative of the slopes in (a) correlates with the fragility steepness index m as shown in (b). (a) and (b) are reproduced from Ref. [31]. (c) Volume changes ΔV_{4-3} with respect to its value at T_g' plotted versus T_g'/T during undercooling the levitated, molten droplet from a temperature far above melting point into the glassy state. The solid line corresponds to the linear fit. Note that its slope $m_{\text{str}}^{(V_{4-3})} = 0.067$ can be transferred into kinetic fragility $m = 65$ corresponding to $D* \sim 12$ as shown by the red arrow in (b). The dashed area in (b) represents the uncertainty of fitting.

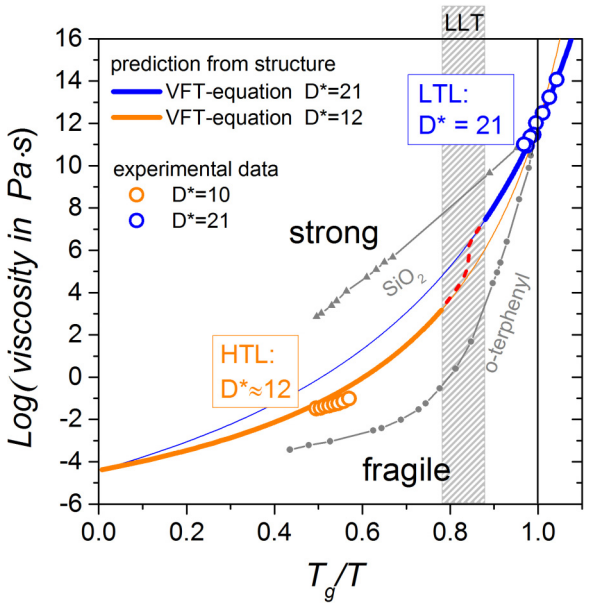

FIG. 6. T_g-scaled Arrhenius plot (Angell plot) of the viscosity behavior derived from the structural data according to the empirical correlation reported in Ref. [31] (solid lines). The predicted trend adequately reproduces the experimentally observed viscous behavior (empty circles). The dashed line connecting the viscosity data of the HTL with the LTL is the hypothesized course during the LLT. For comparison the data for SiO_2 and o-terphenyl taken from Ref. [58] are included.

of the structural data thus predicts a FST associated with the LLT in the deeply undercooled liquid at $T/T_g \sim 1.2$.

A graphical representation of the structure-predicted viscosity behavior in comparison to the experimental data is shown in Fig. 6. The course of viscosity is determined from the structural data by inserting the derived $D*$ values into VFT equation. The high temperature limit $T \to \infty$ corresponding to the preexponential factor η_0 in the VFT equation is calculated as $\eta_0 = \frac{N_A\, h}{V_m}$, where h is Planck's constant, N_A is Avogadro's number, and V_m is the molar volume, based on Eyring's considerations on the lower bound for viscosity [56]. Figure 6 demonstrates that the structure-predicted viscosity behavior adequately describes the experimental data. Furthermore, a two order of magnitude change in viscosity is suggested as illustrated by the hypothesized course of viscosity during the LLT shown as the dashed line in Fig. 6. This agrees with the magnitude of viscosity change throughout a fragile-strong transition determined by Couette viscometry in a different bulk metallic glass forming alloy [57].

IV. CONCLUSION

In conclusion, we report strong evidence for a LLT in the deeply undercooled liquid state at $T/T_g \sim 1.2$ in which a less ordered high temperature phase transforms to a more ordered low temperature phase. Analysis of real space structural data shows that the LLT involves changes in SRO and MRO. Relying on previous observations linking the structural evolution at MRO to fragility it is demonstrated that the changes in MRO correlations on the length scale of about 1 nm can adequately describe the experimentally observed changes in the viscous behavior. As a consequence, a FST accompanied by a 2 order of magnitude change in viscosity is predicted. Our present findings substantiate the idea that MRO correlations are inherently linked to the viscous behavior. This is in line with recent MD simulations which suggest that the viscous slowdown (fragility) of metallic liquids upon undercooling is related to the expansion of MRO by an aggregation or network formation of energetically preferred atomic clusters. The present work corroborates the conception that strong liquids differ from fragile liquids by occupying different flanks of an underlying order-disorder transition as postulated in the "big picture" of glass forming liquids [18,19]. This stresses the role of LLTs and their dynamic implications towards understanding the viscous slowdown towards the glass transition.

ACKNOWLEDGMENTS

The authors gratefully acknowledge technical support from D. Holland-Moritz, C. Yuan, U. Rütt, and O. Gutowski. Parts of this research were carried out at the light source PETRA III at DESY, a member of the Helmholtz Association (HFG). S.W. is partially supported by Alexander von Humboldt Foundation Feodor Lynen Fellowship.

[1] S. Aasland and P. F. McMillan, Nature (London) **369**, 633 (1994).
[2] Y. Katayama, Y. Inamura, T. Mizutani, M. Yamakata, W. Utsumi, and O. Shimomura, Science **306**, 848 (2004).
[3] M. H. Bhat, V. Molinero, E. Soignard, V.C. Solomon, S. Sastry, J. L. Yarger, and C. A. Angell, Nature (London) **448**, 787 (2007).
[4] S. Sastry, Nature (London) **409**, 164 (2001).
[5] L. Xu, S. V. Buldyrev, C. A. Angell, and H. E. Stanley, Phys. Rev. E. **74**, 031108 (2006).
[6] V. Molinero, S. Sastry, and C. A. Angell, Phys. Rev. Lett. **97**, 075701 (2006).
[7] I. Saika-Voivod, P. H. Poole, and F. Sciortino, Nature (London) **412**, 514 (2001).
[8] J. L. Yarger and G. H. Wolf, Science **306**, 820 (2004).
[9] H. W. Sheng, H. Z. Liu, Y. Q. Cheng, J. Wen, P. L. Lee, W. K. Luo, S. D. Shastri, and E. Ma, Nat. Mater. **6**, 192 (2007).
[10] O. Mishima, J. Chem. Phys. **133**, 144503 (2010).
[11] J. R. Errington and P. G. Debenedetti, Nature (London) **409**, 318 (2001).
[12] K. Murat and H. Tanaka, Nat. Mater. **11**, 436 (2012).
[13] M. Hemmati, C. T. Moynihan, and C. A. Angell, J. Chem. Phys. **115**, 6663 (2001).
[14] R. Kurita and H. Tanaka, Science **306**, 845 (2004).
[15] H. Tanaka, R. Kurita, and H. Mataki, Phys. Rev. Lett. **92**, 025701 (2004).
[16] S. Wei, F. Yang, J. Bednarcik, I. Kaban, O. Shuleshova, A. Meyer, and R. Busch, Nat. Commun. **4**, 2083 (2013).
[17] P. H. Poole, T. Grande, C. A. Angell, and P. F. McMillan, Science **275**, 322 (1997).
[18] C. A. Angell, J. Non-Cryst. Solids **354**, 4703 (2008).
[19] C. A. Angell, MRS Bull. **33**, 544 (2008).
[20] C. Zhang, L. Hu, Y. Yue, and J. C. Mauro, J. Chem. Phys. **133**, 014508 (2010).
[21] S. Wei, P. Lucas, and C. A. Angell, J. Appl. Phys. **118**, 034903 (2015).
[22] J. Orava, D. W. Hewak, and L. A. Greer, Adv. Funct. Mater. **25**, 4851 (2015).
[23] C. A. Angell, J. Non-Cryst. Solids **131–133**, 13 (1991).
[24] G. Adam and J. H. Gibbs, J. Chem. Phys. **43**, 139 (1965).
[25] J. C. Mauro, Y. Yue, A. J. Ellison, P. K. Gupta, and D. C. Allan, PNAS **106**, 19780 (2009).
[26] M. Goldstein, J. Chem. Phys. **51**, 3728 (1969).
[27] P. G. Debenedetti and F. H. Stillinger, Nature (London) **410**, 259 (2001).
[28] T. Hecksher, A. I. Nielsen, N. B. Olsen, and J. C. Dyre, Nat. Phys. **4**, 737 (2008).
[29] L.-M. Martinez and C. A. Angell, Nature (London) **410**, 663 (2001).
[30] I. Gallino, J. Schroers, and R. Busch, J. Appl. Phys. **108**, 063501 (2010).
[31] S. Wei, M. Stolpe, O. Gross, Z. Evenson, I. Gallino, W. Hembree, J. Bednarcik, J. J. Kruzic, and R. Busch, Appl. Phys. Lett. **106**, 181901 (2015).
[32] Z. Evenson, T. Schmitt, M. Nicola, I. Gallino, and R. Busch, Acta Mater. **60**, 4712 (2012).
[33] T. Kordel, D. Holland-Moritz, F. Yang, J. Peters, T. Unruh, T. Hansen, and A. Meyer, Phys. Rev. B **83**, 104205 (2011).
[34] See Supplemental Material at http://link.aps.org/supplemental/10.1103/PhysRevB.93.014201 for descriptions of the sample preparation, instrumental setup, experimental conduct, data analysis, thermal expansion data, and the magnified plots of the real space structural changes.
[35] C. C. Hays, J. Schroers, W. L. Johnson, T. J. Rathz, R. W. Hyers, J. R. Rogers, and M. B. Robinson, Appl. Phys. Lett. **79**, 1605 (2001).
[36] I. Gallino, M. B. Shah, and R. Busch, Acta Mater. **55**, 1367 (2007).
[37] G. N. Greaves, M. C. Wilding, S. Fearn, D. Langstaff, F. Kargl, S. Cox, Q. Vu Van, O. Maj'erus, C. J. Benmore, R. Weber, C. M. Martin, and L. Hennet, Science **322**, 566 (2008).
[38] A. R. Yavari, A. Moulec, A. Inoue, N. Nishiyama, N. Lupu, E. Matsubara, W. B. Botta, G. Vaughan, M. Michiel, and A. Kvick, Acta Mater. **53**, 1611 (2005).
[39] Z. Evenson, I. Gallino, and R. Busch, J. Appl. Phys. **107**, 123529 (2010).
[40] J. C. Bendert, M. E. Blodgett, A. K. Gangopadhyay, and K. F. Kelton, Appl. Phys. Lett. **102**, 211913 (2013).
[41] H. B. Lou, X. D. Wang, Q. P. Cao, D. X. Zhang, J. Zhang, T. Hu, H. K. Mao, and J. Z. Jiang, Proc. Natl. Acad. Sci. USA **110**, 10068 (2013).
[42] A. K. Gangopadhyay, M. E. Blodgett, M. L. Johnson, J. McKnight, V. Wessels, A. J. Vogt, N. A. Mauro, J. C. Bendert, L. Yang, and K. F. Kelton, J. Chem. Phys. **140**, 044505 (2014).
[43] J. Ding, M. Xu, P. F. Guan, S. W. Deng, Y. Q. Cheng, and E. Ma, J. Chem. Phys. **140**, 064501 (2014).
[44] S. G. Hao, C. Z. Wang, M. J. Kramer, and K. M. Ho, J. Appl. Phys. **107**, 053511 (2010).
[45] T. Schenk, D. Holland-Moritz, V. Simonet, R. Bellissent, and D. M. Herlach, Phys. Rev. Lett. **89**, 075507 (2002).
[46] H. Tanaka, J. Non-Cryst. Solids **351**, 678 (2005).
[47] A. Hirata, L. J. Kang, T. Fujita, B. Klumov, K. Matsue, M. Kotani, A. R. Yavari, and M. W. Chen, Science **341**, 376 (2013).
[48] R. Soklaski, Z. Nussinov, Z. Markow, K. F. Kelton, and L. Yang, Phys. Rev. B **87**, 184203 (2013).
[49] S. G. Hao, C. Z. Wang, M. Z. Li, R. E. Napolitano, and K. M. Ho, Phys. Rev. B **84**, 064203 (2011).
[50] J. Ding, Y.-Q. Cheng, H. Sheng, and E. Ma, Phys. Rev. B **85**, 060201 (2012).
[51] L. Ward, D. Miracle, W. Windl, O. N. Senkov, and K. Flores, Phys. Rev. B **88**, 134205 (2013).

[52] Y. Zhang, F. Zhang, C. Z. Wang, M. I. Mendelev, M. J. Kramer, and K. M. Ho, Phys. Rev. B **91**, 064105 (2015).
[53] N. A. Mauro, M. Blodgett, M. L. Johnson, A. J. Vogt, and K. F. Kelton, Nat. Commun. **5**, 4616 (2014).
[54] D. B. Miracle, Nat. Mater. **3**, 697 (2004).
[55] R. Böhmer, K. L. Ngai, C. A. Angell, and D. J. Plazek, J. Chem. Phys. **99**, 4201 (1993).
[56] H. Eyring, J. Chem. Phys. **4**, 283 (1936).
[57] C. Way, P. Wadhwa, and R. Busch, Acta Mater. **55**, 2977 (2007).
[58] C. A. Angell, Science **267**, 1924 (1995).